Supporting Information for "Computation-guided discovery of influenza endonuclease inhibitors"

Eric Chen,[a‡] Robert V. Swift,[a‡] Nazilla Alderson,[b] Victoria A. Feher[a], Gen-Sheng Feng,[b] and Rommie E. Amaro*[a]

[a]Department of Chemistry and Biochemistry, University of California San Diego, La Jolla, California, 92093, United States of America. [b]Department of Pathology, University of California San Diego, La Jolla, California, 92093, United States of America.

Pharmacophore Generation & Vetting

PDB IDs 4E5F, 4AWF, 4E5H, 4E5I, 4E5J, 4AWK, 4AVG, 4AWG (chain A), and 4AWM were downloaded from the protein databank. Ligand, or inhibitor, structures were aligned in two stages. First, the RMSD between alpha-carbon atoms was minimized using the RMSD Trajectory Tool in VMD (1). The ligands from the aligned endonuclease structures were then exported to individual PDB files and imported into Schrödinger's Maestro (2). After the files were read, metal binding oxygen atoms were aligned using the superposition tool in Schrödinger's Maestro. PDB files containing the nine aligned ligands were saved and imported into OpenEye's vROCS (3). Pharmacophore models were generated using the vROCS query wizard. The max molecules per model was set to 3, and the number of models to keep was set to 5. This resulted in 5 pharmacophores, each of which was constructed from three different ligands. The top five pharmacophores returned by vROCS were considered without further modifications.

To evaluate the performance of each pharmacophore model, 6 inhibitors not contained in the pharmacophore were seeded into the National Cancer Institutes Diversity Set III (NCIDSIII), which was downloaded from (http://dtp.nci.nih.gov/branches/dscb/div2_explanation.html) in sdf format (we note that the diversity set III has since been replaced by the diversity set IV). To compare model performance, vROCs was used in validation mode. The validation mode requires two oeb files (Open Eye Binary), one that stores a conformational ensemble of a set of known "actives," or endonuclease inhibitors, and another that stores a conformational ensemble of a set of "decoys," or non-binders. The conformational ensemble of the decoys was generated from the NCIDSIII sdf file using OpenEye's OMEGA program (4) with default settings. The inhibitor sdf files were generated using the build tools in Schrödinger's Maestro. The inhibitors were always taken as the co-crystalized compounds not included in the pharmacophore model being tested. For example, for a pharmacophore generated from the ligands in structures with PDB IDs 4E5H, 4E5J, and 4AWG, the "actives" were taken as the ligands in the crystal structures with PDB IDs 4E5F, 4AWF, 4E5I, 4AWK, 4AVG, 4AWM. Using Tanimoto combination scoring, each model was used to screen each validation database and produce a receiver operating characteristic curve (ROC curve) (5). The area under the ROC curve, or AUC was also calculated. The AUC value is equivalent to the probability that the model will rank an inhibitor ahead of a non-inhibitor if the two are randomly chosen (5) and was used to compare the relative performance of each model. The model with the largest AUC value was selected for subsequent screening.

Library Filtering

The ChemBridge Express Pick library was downloaded as a set of two-dimensional sdf files from the ChemBridge website immediately following their September 2012 monthly update. The database was filtered using OpenEye's FILTER (6). The OpenEye "lead filter" rules were applied with the following modifications: compounds with molecular weight between 250 and 460 a.m.u with fewer than 10 rotatable bonds were retained; salts & duplicate structures were removed; both predicted and known aggregators were removed; compounds predicted to be "poorly" soluble or worse were discarded; compounds with 3 or more (out of 5) violations of Lipinski's rules (7) were removed. Following compound filtering, three-dimensional structures, as well as a conformation library was generated for each compound using OpenEye's OMEGA program with default settings.

Library Virtual Screening

Following compound library filtering, structure and conformation generation, the virtual screen was performed on TACC Ranger, an XSEDE resource (https://www.xsede.org), which has since been decommissioned. Compounds were ranked according to their TanimotoCombo coefficients. While the pharmacophore reasonably delineated the steric requirements imposed by the endonuclease active site, as a result of the complexity of the descriptor points, metal binding groups were not prioritized. To increase the

probability of hit discovery, the top ten thousand compounds were manually inspected, and compounds with likely metal binding scaffolds were removed for purchase. Roughly, a metal binding scaffold was defined as two or three keto or hydroxyl oxygen atoms that overlapped with any of the donor/acceptor descriptor points adjacent to the manganese atoms (Fig. 1a). The two lead authors carried out the inspection process over the course of 3 days by displaying each compound aligned in the pharmacophore in OpenEye's visualization program, Vida. Two hundred and thirty seven compounds with putative metal binding groups were retained for purchase.

Protein Production and Purification

Dr. Takashi Kuzuhara kindly provided the H1N1 PA_N plasmid (8). The plasmids were transformed into *E. coli* strain BL21(DE3) (Life Technology). 0.2 mM isopropyl β-D-1-thiogalactopyranoside (IPTG) was added to induce protein expression for 7 hr at 37^0C when bacteria culture O.D.(A600) reached 0.7. PA_N was tagged with 6xHis and the protein was purified by His-Trap HP affinity column(GE). PA_N was purified to near homogeneity, confirmed by protein gel electrophoresis to be a single band at about 24 kD. Purified protein was aliquoted and stored at -80^0C.

Endonuclease Assays

Assays were conducted as described in (9,10). A seventeen base single-stranded DNA oligonucleotide substrate, dual-labeled with 5'-FAM donor fluorophore and 3'-TAMRA quencher (FAM-AAT CGC AGG CAG CAC TC-TAM), was synthesized (Integrated DNA Technologies, Inc.) and used as a reporter. Endonuclease cleavage separates the fluorophore and quencher, increasing fluorescence, and the ability of each compound to inhibit this activity was monitored. The assay can be conducted in 96 or 384 well format for reasonably high throughput screening. To construct dose response curves, compounds were mixed at various concentrations with 1μM PA_N and 0.5μM oligo substrate in either 96 or 384-well plates at 100μl and 30μl, respectively. To reduce the chance of getting promiscuous hits, 0.2% Triton X-100 was included in the assay buffer (20mM Tris pH8, 150 mM NaCl, 2mM MnCl2, 10 mM β-mercaptoethanol). Epigallocatechin 3-gallate (EGCG) from green tea (Sigma) was used as a positive control. Test compounds were dissolved in DMSO, and DMSO was used as the vehicle control. Fluorescence was read at 485 nm excitation and 535 nm wavelengths in the BioTek plate reader, Flx-800. Recordings were made at 37^0C for 30min at 1min intervals, and the rate, Vm, was calculated using the BioTek KC4 software. IC_{50} values were determined from the dose response curves with nonlinear curve fitting using GraphPad software. Characteristic dose response curves for compounds 2 and 4 are give in figure S1.

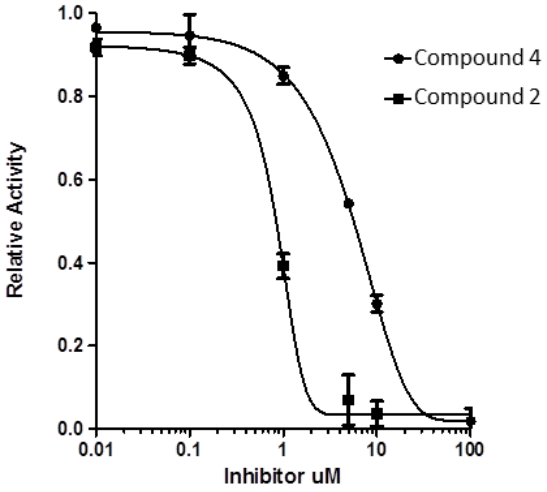

Figure S1. Dose response curves of Compound 2 and 4 inhibiting PA endonuclease activity from FRET based assays. The assays were carried out in the presence of various concentrations of test compounds or vehicle control. Velocity (V_m) of the reactions was obtained from the fluorescence plate readers and normalized to V_m in the absence of the inhibitors to calculate the Relative Activity. IC50 values were determined from the dose response data using GraphPad software.

Cytotoxicity Assays

A methylene blue staining assays was used to monitor compound cell toxicity. $1.5x10^4$ Madin-Darby canine kidney (MDCK) cells (ATCC) in 100 µl were plated to each well of a 96-well plate. One day after, compounds at various concentrations in 100µl media were added and incubated for 48 hours, followed by staining with methylene blue dye. DMSO was used as the vehicle control. The plates were read at 630nm wavelength on a plate reader, and the methylene blue staining intensity correlates with cell numbers in the wells. The CC_{50} values reported are the compound concentrations causing 50% of the cell number reduction compared to vehicle control.

Antiviral Assays

Compounds were mixed with virus and added to MDCK cells before fixing and staining with methylene blue. The IC_{50} of the compounds to inhibit virus-induced cytopathic effect were determined as described with modifications (10). Tissue culture plates (96-well) were seeded with 1.5×10^4 cells/well and incubated for 24 h at 37°C under 5% CO2. The cells were washed twice with PBS and then infected with Influenza A H1N1 (A/Puerto Rico/8/1934) at MOI 0.01 in 100 µl of DMEM with or without varying concentrations of test compounds. Cells without any virus were included as a control. After incubation at 37°C for 48 h, cells were fixed in ethanol, stained with methylene blue dye, and the plates were read at 630nm wavelength on a plate reader. Alternatively, cell viability was determined by using a luminescence based CellTiter-Glo assay (Promega) according to the manufacturer's instructions. IC_{50} values were determined from dose response curves.

Conformational Analysis & Butanamide Internal Strain

The N-1,4-diphenyl-2,4-dioxobutanamide enolate was prepared using the build tools in Schrödinger's Maestro. A two dimensional coordinate scan was performed in MacroModel (11) along the φ_1 and φ_2 torsions illustrated in figure S2. Energy was evaluated every 10^o along a 360^o interval for each torsion. The 2005 OPLS force field was used in an implicit GBSA water solvent with no dielectric cutoff. Prior to energy evaluation at each point in torsion space, a 1500 step Polak-Ribiere conjugate gradient minimization was performed. Following the coordinate scan, the relative energies of each conformation were examined and the lowest energy conformer ($\varphi_1 = 180^o$, $\varphi_2 = 30^o$) was identified (Figure S2 A & B). Each conformer was also visually compared, and a likely metal binding conformer (Figure S2 C) was identified ($\varphi_1 = 180^o$, $\varphi_2 = 30^o$). Using the OPLS FF and implicit GBSA solvent described above, the energy difference between these two conformations is 5.6 kcal/mol.

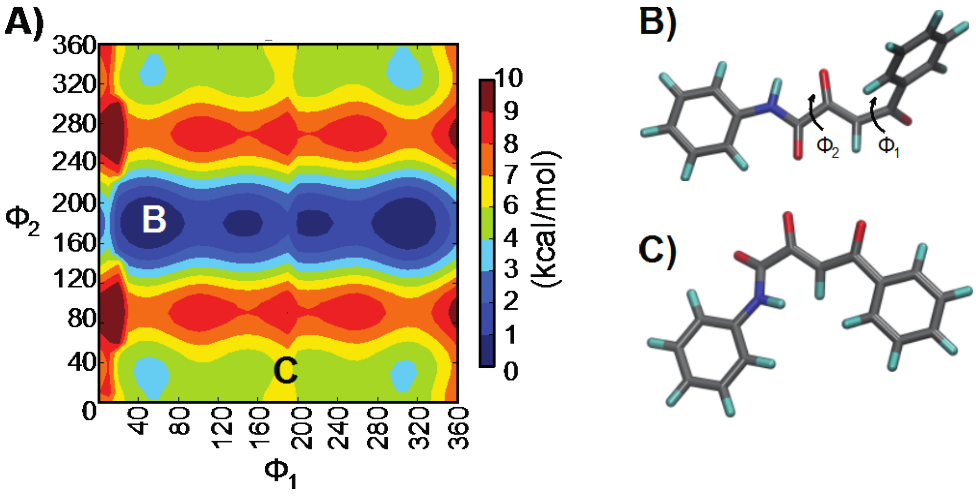

Figure S2. 2,4-dioxobutanamide conformational analysis. A) A two-dimensional potential energy surface calculated along the φ_1 and φ_2 dihedral angles (illustrated in B) using the 2005 OPLS force field and an generalized born implicit water model. A bold white "B" indicates the location of the minimum energy conformation, shown in B). The location of the likely metal binding conformation, shown in C), is indicated by a bold black "C."

Both the minimum energy and metal binding conformers were minimized in Gaussian09 (12) using the opt keyword, MP2 theory, the 6-31+G(d,p) basis set, and the default implicit water model. While quantum mechanical optimization did not significantly change compound geometry (Figure S3), the energy difference was found to be 3.7 kcal/mol, with the metal binding conformation the higher energy species. Collectively, these analyses indicate that upon binding, the compound incurs a 3.7 – 5.6 kcal/mol internal strain penalty.

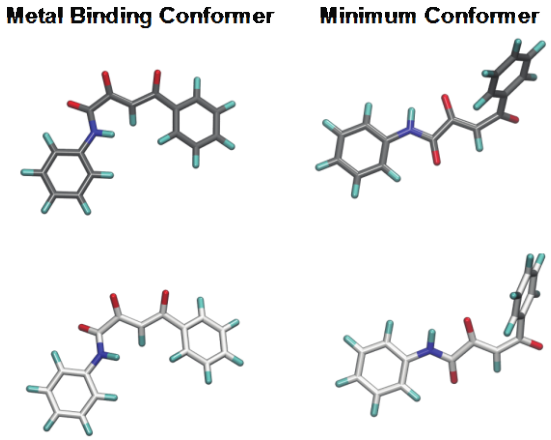

Figure S3. **Comparison of the classically and quantum mechanically determined conformer geometries**. The carbon atoms in the classically determined conformers (2005 OPLS FF in GBSA water) are colored gray, while the carbon atoms in the quantum mechanically determined conformers (MP2 6-31+G(d,p) PCM implicit water) are colored white. Quantum mechanical minimization was carried out from the classically determined conformers found in the two-dimensional conformational analysis described in Figure S2. The metal binding conformers are shown in the column on the left, while the minimum energy conformations are shown in the column on the right. The all-atom RMSD between the metal binding conformers is 0.24Å, while the all-atom RMSD between the minimum conformers is 0.43Å.

Compound-Pharmacophore Alignment and Docking

Pharmacophore alignment was performed as described in the "Library Virtual Screening" section, above. Several steps of preparation were performed to carry out docking. An sdf file of compounds **1**, **4**, **6**, **11**, and **13**, the most potent endonuclease inhibitors in each compound class, were downloaded from the hit2lead website (hit2lead.com). The sdf files were converted to three-dimensional structures using the Protein Preparation Wizard (13) in Schrödinger's Maestro. The MarvinSketch protonation calculator plugin (14) was then used to estimate pKa values for each compound, and these values were used to guide the preparation of different ionization and tautomer states used for docking. To reduce the complexity of the problem, only the mono-anion of each compound was considered. Each state was manually generated from the initial three-dimensional structures using the molecular editing tools available in Maestro's build tool bar. The predicted pKa values and the ionization and tautomer states that were prepared for docking are illustrated in figure S4.

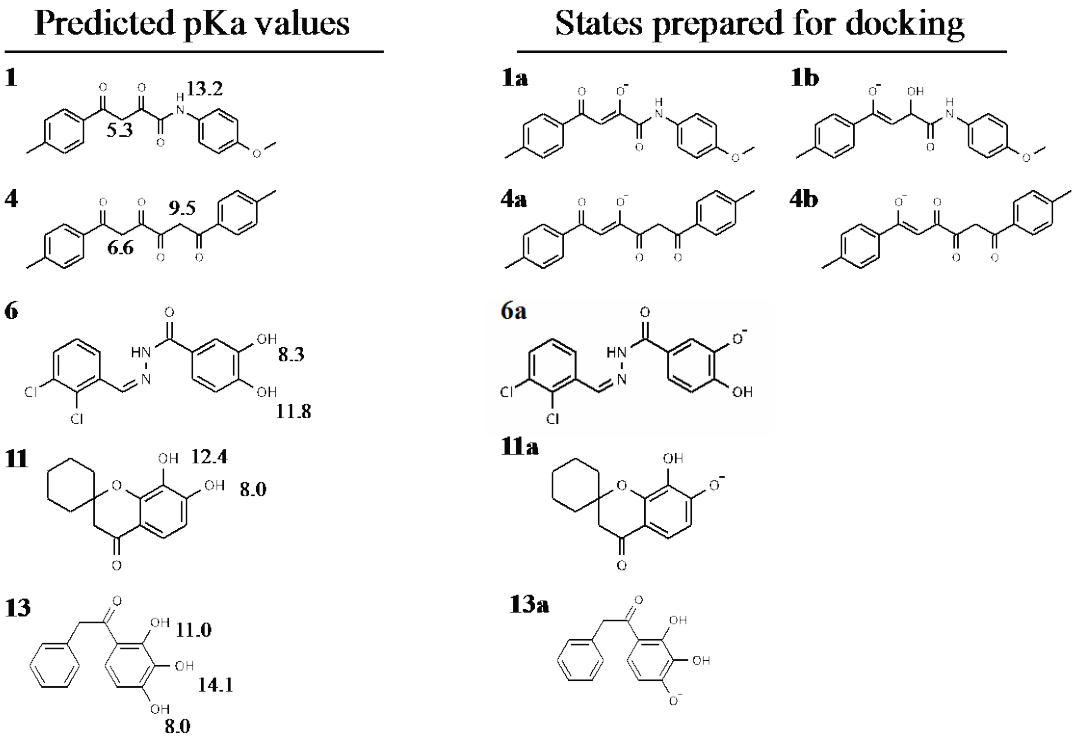

Figure S4. Predicted pKa values and states prepared for docking the most potent inhibitor of each compound class. Compound numbers are shown in bold and correspond to those listed in tables 1 through 5. In the column on the left, predicted pKa values are listed adjacent to the corresponding hydrogen atom. In the column on the right, the states prepared for docking are listed with lower case letters denoting unique states.

Docking was carried using Schrödinger's Glide (15). To simplify the docking analysis, docking was performed to chain A of PDB ID 4AVG. Globally, the conformation of the active-site residues is similar across the published endonuclease crystal structures, and other crystal structures may also produce reasonable results. We focused on 4AVG because it is bound to a 2,4-dioxobutanoic acid like inhibitor with a nM Ki that is similar to two of the five compound classes found (the dioxobutanamides presented in Table 1, and the hexanetetrones presented in Table 2). The protein structure was imported into Maestro and prepared using the Protein Preparation Wizard. With the exception of a manganese-coordinating water, which leaves the expected ligand-binding mode unobstructed, all crystallographic water molecules were deleted. A positive-two-charge and a "M2" MacroModel atom type were manually assigned to each manganese atom. A pH of 7 was specified, and the Protein Preparation Wizard automatically assigned all other charge states and atom types. Using the refine tab in the Protein Preparation Wizard, the hydrogen bond network was optimized, completing receptor preparation. Following receptor preparation, docking grids were produced using the Receptor Grid Generation tool in Maestro. The grid center was positioned on the centroid of the crystalized ligand. The inner box was set to 10 $Å^3$ while the outer box was set to 25.8 $Å^3$. All other grid generation parameters were set to their default values. Following grid preparation, docking was performed using the SP scoring function on each of the states illustrated in figure S4. The top 5 poses were retained for each docking state, and the default values of all other parameters were retained.

The pharmacophore alignment and docking-predicted bound state are shown in figures S5 through S9. Images of the compounds and the compounds aligned in the pharmacophore were created using OpenEye's Vida (16), while images of the docked poses were created in VMD (3). The images of the docking poses are roughly oriented as in Figure 4 from Dubois et al (9).

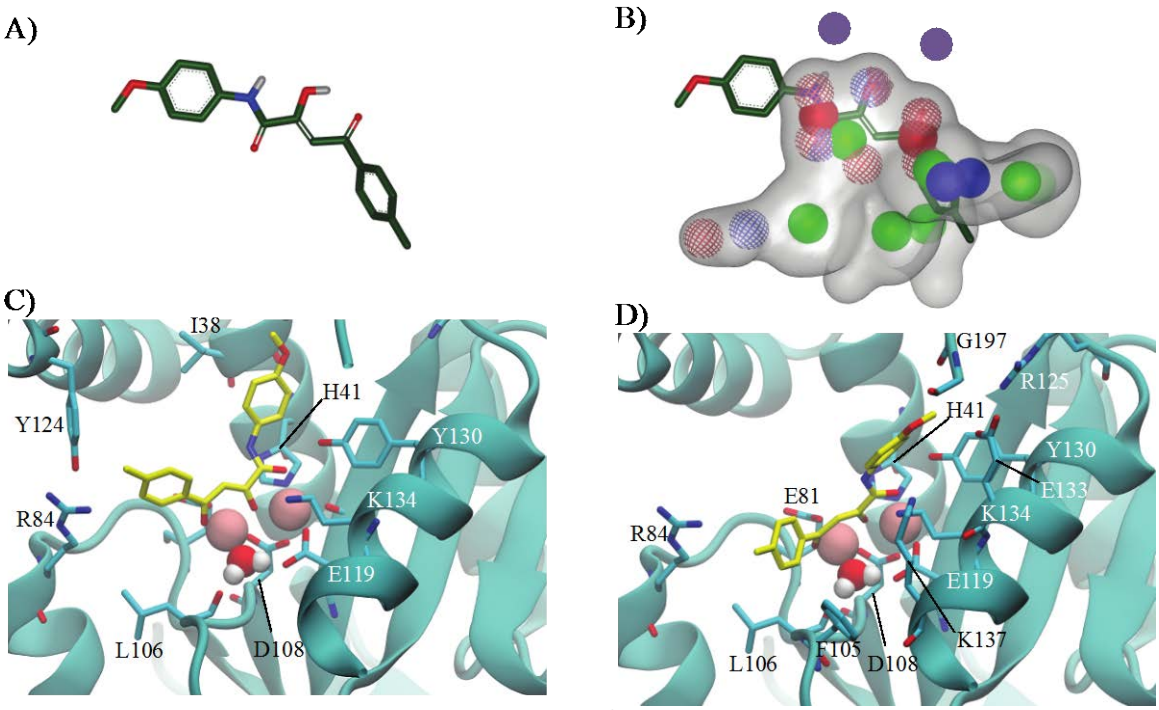

Figure S5. Compound-pharmacophore alignment and docking of compound 1. A) Compound **1** is rendered in sticks. Carbon atoms are colored dark green, nitrogen atoms are colored blue, oxygen atoms are colored red, and hydrogen atoms are colored white. B) The best alignment of compound **1** with the pharmacophore. Compound **1** is colored as in A). Pharmacophore model volume is represented by a transparent gray surface. Blue, red and red/blue wire frame spheres represent hydrogen bond donors, acceptors and acceptors/donors, respectively. Green, red and blue spheres represent ring centers, anions, and cations, respectively. Magenta spheres, not a pharmacophore model element, represent the position of the active-site manganese. C) First predominant bound state predicted by docking state **1a** (figure S4). D) First predominant bound state predicted by docking state **1b** (figure S4). In both C) and D), compound **1** is shown in sticks, carbon atoms are colored yellow, oxygen atoms are colored red, and nitrogen atoms are colored blue. Protein secondary structure is rendered in cartoon, while residues within 4 Å of compound **1** are rendered as sticks with carbon atoms colored cyan, nitrogen atoms colored blue, and oxygen atoms colored red. Two manganese ions and a coordinating water are rendered as Van der Waals spheres. The manganese ions are colored pink, the water oxygen atom is colored red, and the water hydrogen atoms are colored white.

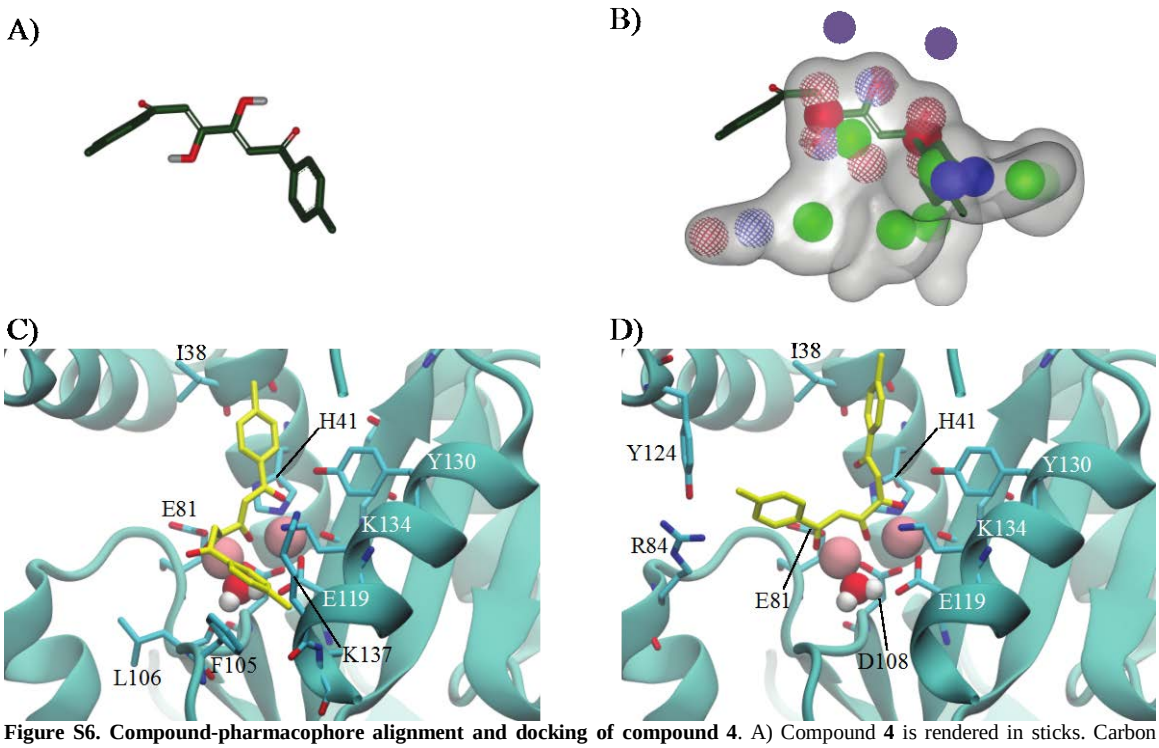

Figure S6. Compound-pharmacophore alignment and docking of compound 4. A) Compound **4** is rendered in sticks. Carbon atoms are colored dark green, nitrogen atoms are colored blue, oxygen atoms are colored red, and hydrogen atoms are colored white. B) The best alignment of compound **4** with the pharmacophore. Compound **4** is colored as in A). Pharmacophore model volume is represented by a transparent gray surface. Blue, red and red/blue wire frame spheres represent hydrogen bond donors, acceptors and acceptors/donors, respectively. Green, red and blue spheres represent ring centers, anions, and cations, respectively. Magenta spheres, not a pharmacophore model element, represent the position of the active-site manganese. C) First predominant bound state predicted by docking state **4a** (figure S4). D) First predominant bound state predicted by docking state **4b** (figure S4). In both C) and D), compound **4** is shown in sticks, carbon atoms are colored yellow, oxygen atoms are colored red, and nitrogen atoms are colored blue. Protein secondary structure is rendered in cartoon, while residues within 4 Å of compound **4** are rendered as sticks with carbon atoms colored cyan, nitrogen atoms colored blue, and oxygen atoms colored red. Two manganese ions and a coordinating water are rendered as Van der Waals spheres. The manganese ions are colored pink, the water oxygen atom is colored red, and the water hydrogen atoms are colored white.

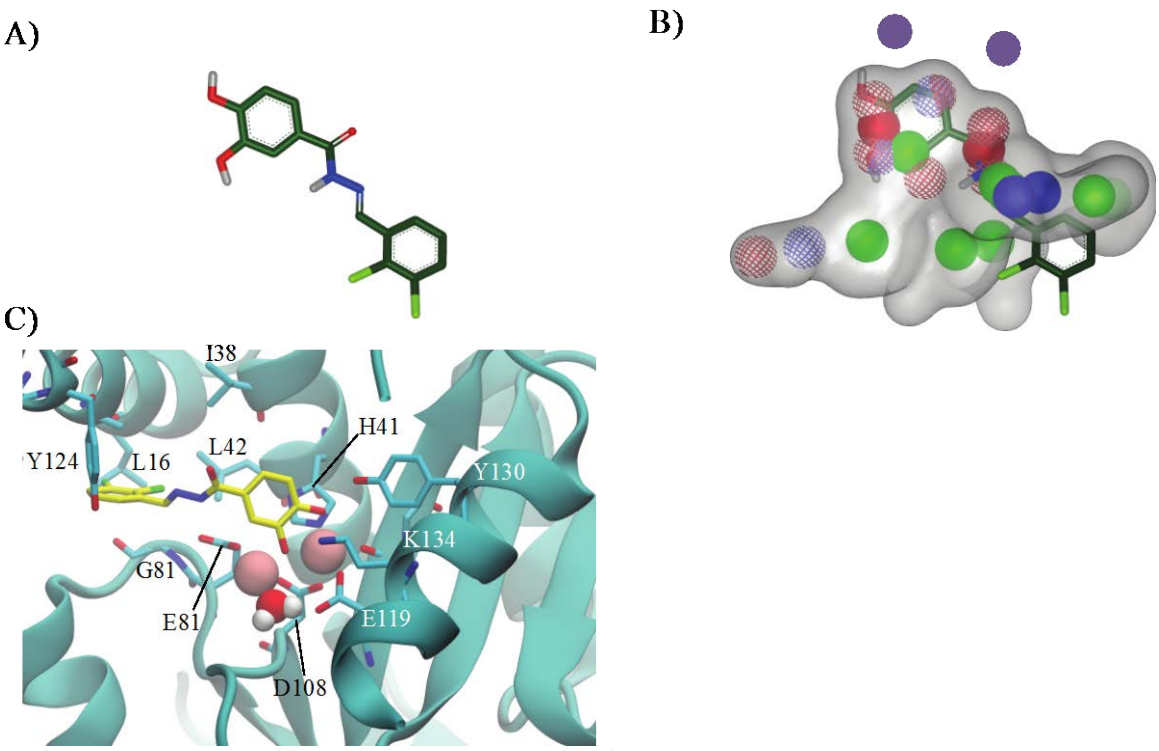

Figure S7. Compound-pharmacophore alignment and docking of compound 6. A) Compound **6** is rendered in sticks. Carbon atoms are colored dark green, nitrogen atoms are colored blue, oxygen atoms are colored red, and hydrogen atoms are colored white. B) The best alignment of compound **6** with the pharmacophore. Compound **6** is colored as in A). Pharmacophore model volume is represented by a transparent gray surface. Blue, red and red/blue wire frame spheres represent hydrogen bond donors, acceptors and acceptors/donors, respectively. Green, red and blue spheres represent ring centers, anions, and cations, respectively. Magenta spheres, not a pharmacophore model element, represent the position of the active-site manganese. C) Predominant bound state predicted by docking state **6a** (figure S4). In C), compound **6** is shown in sticks, carbon atoms are colored yellow, oxygen atoms are colored red, nitrogen atoms are colored blue, and chlorine atoms are colored in green. Protein secondary structure is rendered in cartoon, while residues within 4 Å of compound **6** are rendered as sticks with carbon atoms colored cyan, nitrogen atoms colored blue, and oxygen atoms colored red. Two manganese ions and a coordinating water are rendered as Van der Waals spheres. The manganese ions are colored pink, the water oxygen atom is colored red, and the water hydrogen atoms are colored white.

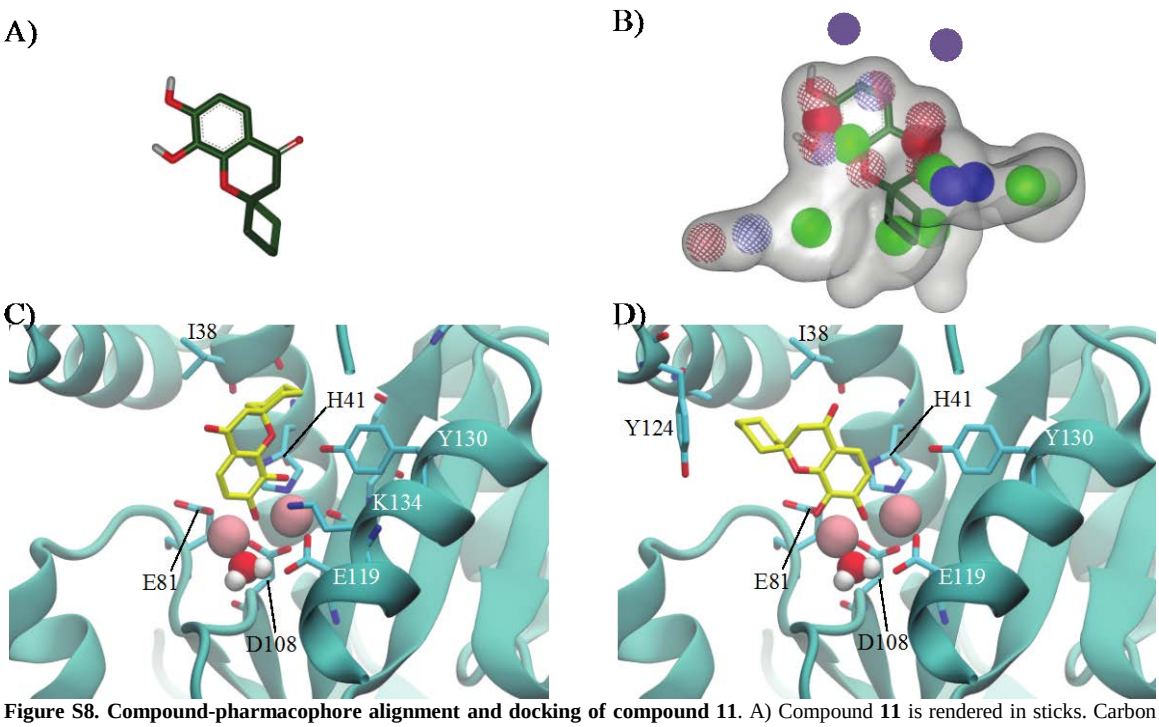

Figure S8. Compound-pharmacophore alignment and docking of compound 11. A) Compound **11** is rendered in sticks. Carbon atoms are colored dark green, nitrogen atoms are colored blue, oxygen atoms are colored red, and hydrogen atoms are colored white. B) The best alignment of compound **11** with the pharmacophore. Compound **11** is colored as in A). Pharmacophore model volume is represented by a transparent gray surface. Blue, red and red/blue wire frame spheres represent hydrogen bond donors, acceptors and acceptors/donors, respectively. Green, red and blue spheres represent ring centers, anions, and cations, respectively. Magenta spheres, not a pharmacophore model element, represent the position of the active-site manganese. C) Predominant bound state predicted by docking state **11a** (figure S4). D) Next highest scoring state using state **11a** (figure S4). In C) and D), compound **11** is shown in sticks, carbon atoms are colored yellow, and oxygen atoms are colored red. Protein secondary structure is rendered in cartoon, while residues within 4 Å of compound **11** are rendered as sticks with carbon atoms colored cyan, nitrogen atoms colored blue, and oxygen atoms colored red. Two manganese ions and a coordinating water are rendered as Van der Waals spheres. The manganese ions are colored pink, the water oxygen atom is colored red, and the water hydrogen atoms are colored white.

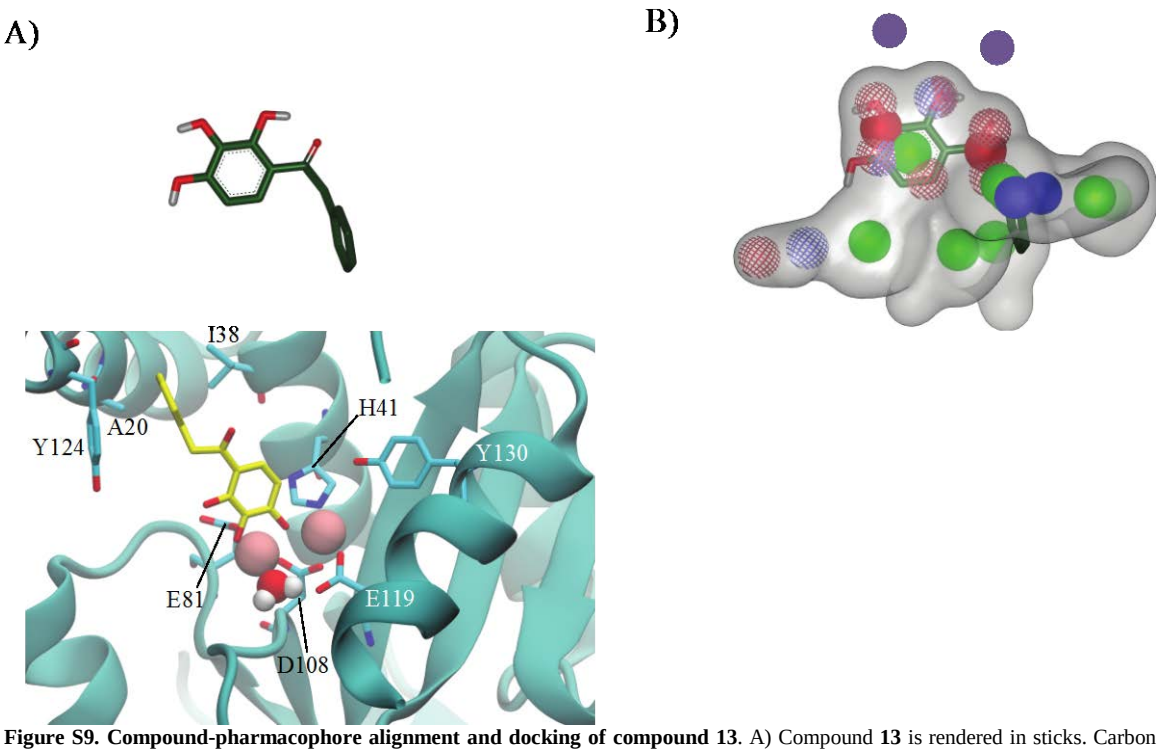

Figure S9. Compound-pharmacophore alignment and docking of compound 13. A) Compound **13** is rendered in sticks. Carbon atoms are colored dark green, nitrogen atoms are colored blue, oxygen atoms are colored red, and hydrogen atoms are colored white. B) The best alignment of compound **13** with the pharmacophore. Compound **13** is colored as in A). Pharmacophore model volume is represented by a transparent gray surface. Blue, red and red/blue wire frame spheres represent hydrogen bond donors, acceptors and acceptors/donors, respectively. Green, red and blue spheres represent ring centers, anions, and cations, respectively. Magenta spheres, not a pharmacophore model element, represent the position of the active-site manganese. C) Predominant bound state predicted by docking state **13a** (figure S4). In C), compound **13** is shown in sticks, carbon atoms are colored yellow, oxygen atoms are colored red, and nitrogen atoms are colored blue. Protein secondary structure is rendered in cartoon, while residues within 4 Å of compound **13** are rendered as sticks with carbon atoms colored cyan, nitrogen atoms colored blue, and oxygen atoms colored red. Two manganese ions and a coordinating water are rendered as Van der Waals spheres. The manganese ions are colored pink, the water oxygen atom is colored red, and the water hydrogen atoms are colored white.

Compound spectra, provided by ChemBridge, are shown in Figures S10 through 25. NMR 1H spectra were obtained using Bruker spectrometers AM400, AMX400, and AC300, operating at 400 or 300 MHz, in DMSO-d6 and CDCl3 solutions. HPLC/MS were performed on Agilent Technologies systems 1100 MSD VLSeries with APCI or ES ionization, equipped with DAD and ELSD PL-ELS 1000/2100 (Polymer Laboratories) and SEDEX LT-ELSD85 (Sedere). Analytical separations were carried out on a 50x4.6mm Onyx C18 (Phenomenex) column or Chromolith SpeedROD RP-18e (Merck KGaA) columns at a flow rate of 3.75mL/min in gradient H2O/CH3CN or MeOH with addition of 0.1% TFA.

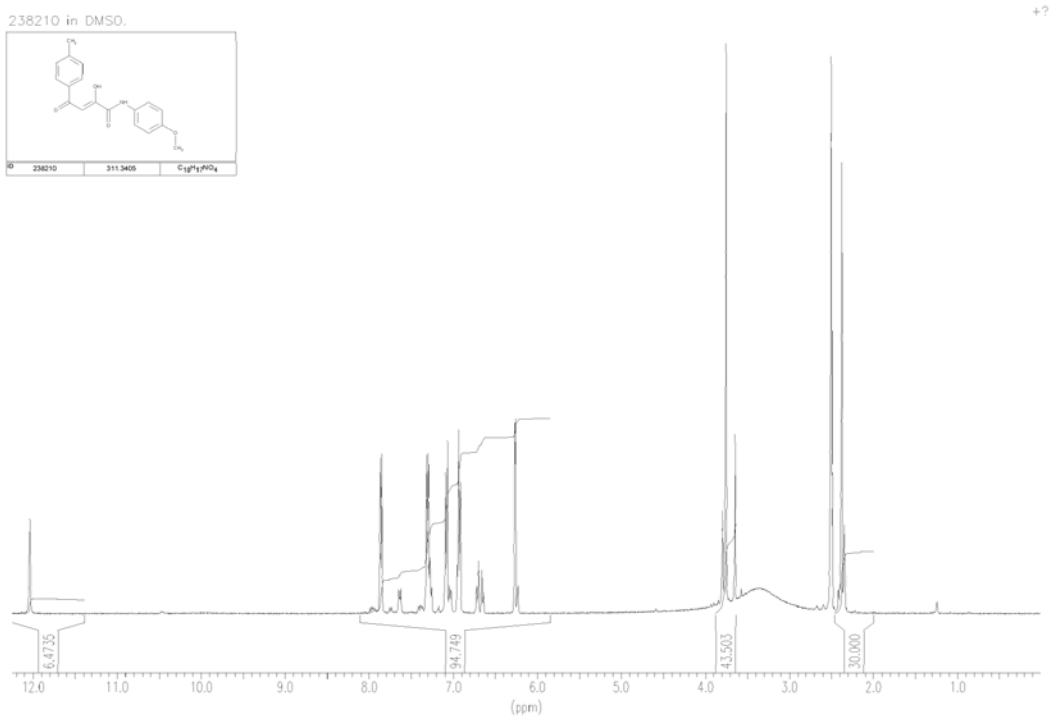

Figure S10. Compound 1

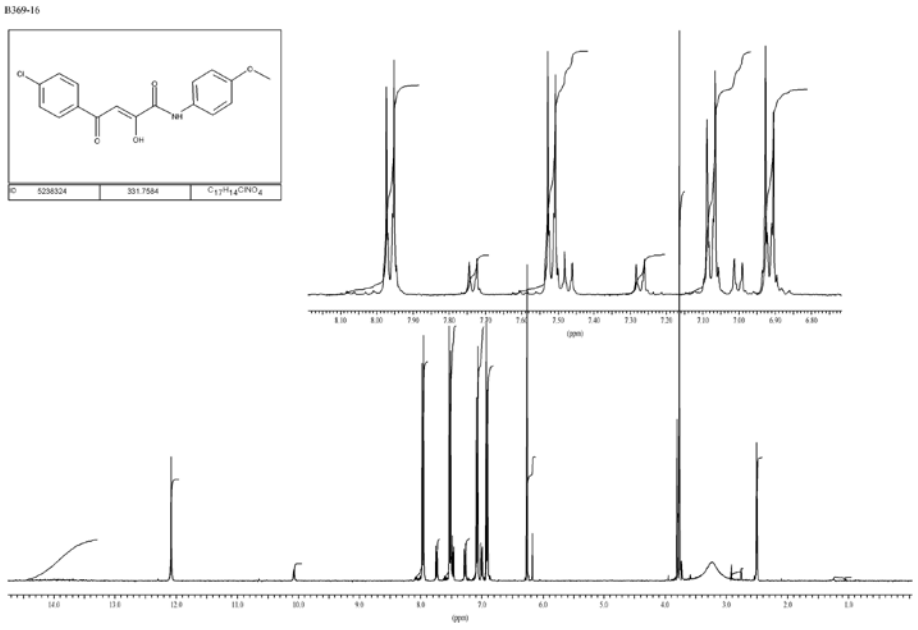

Figure S11. Compound 2

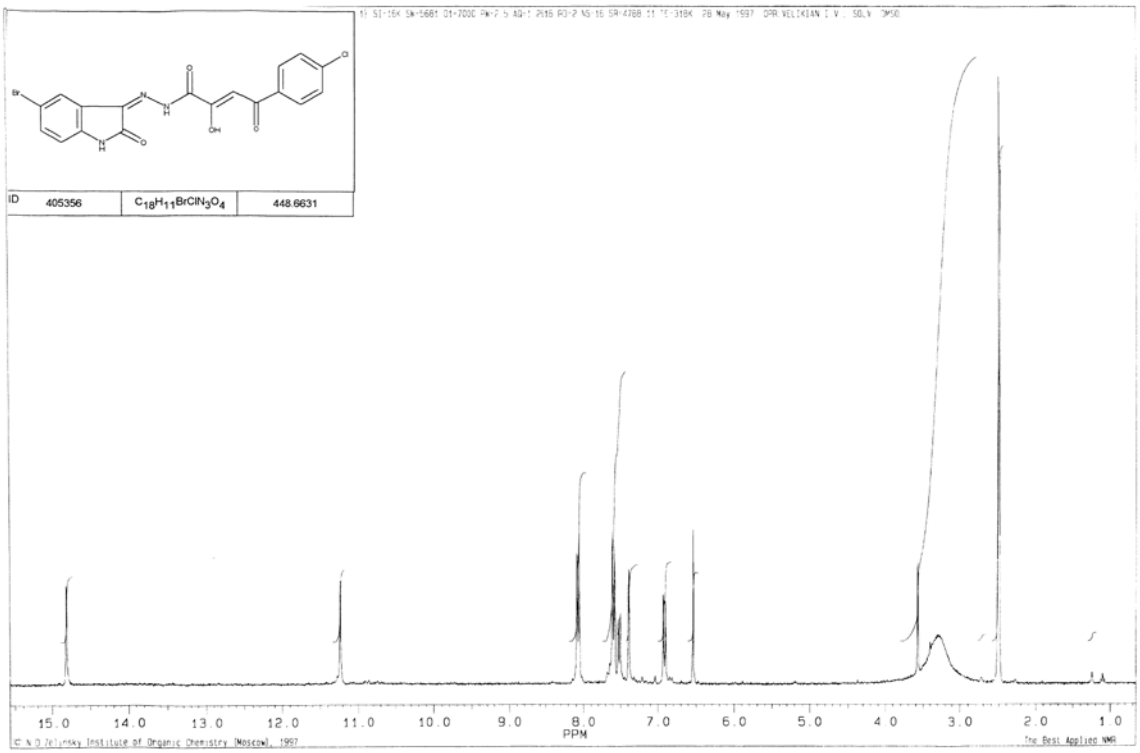

Figure S12. Compound 3

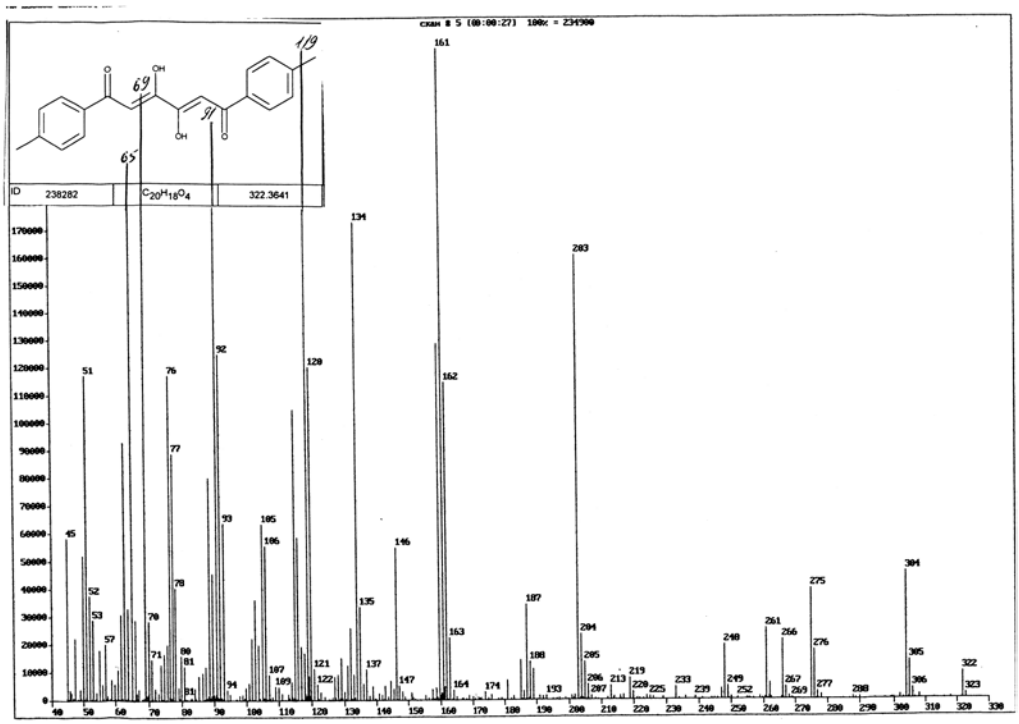

Figure S13. Compound 4

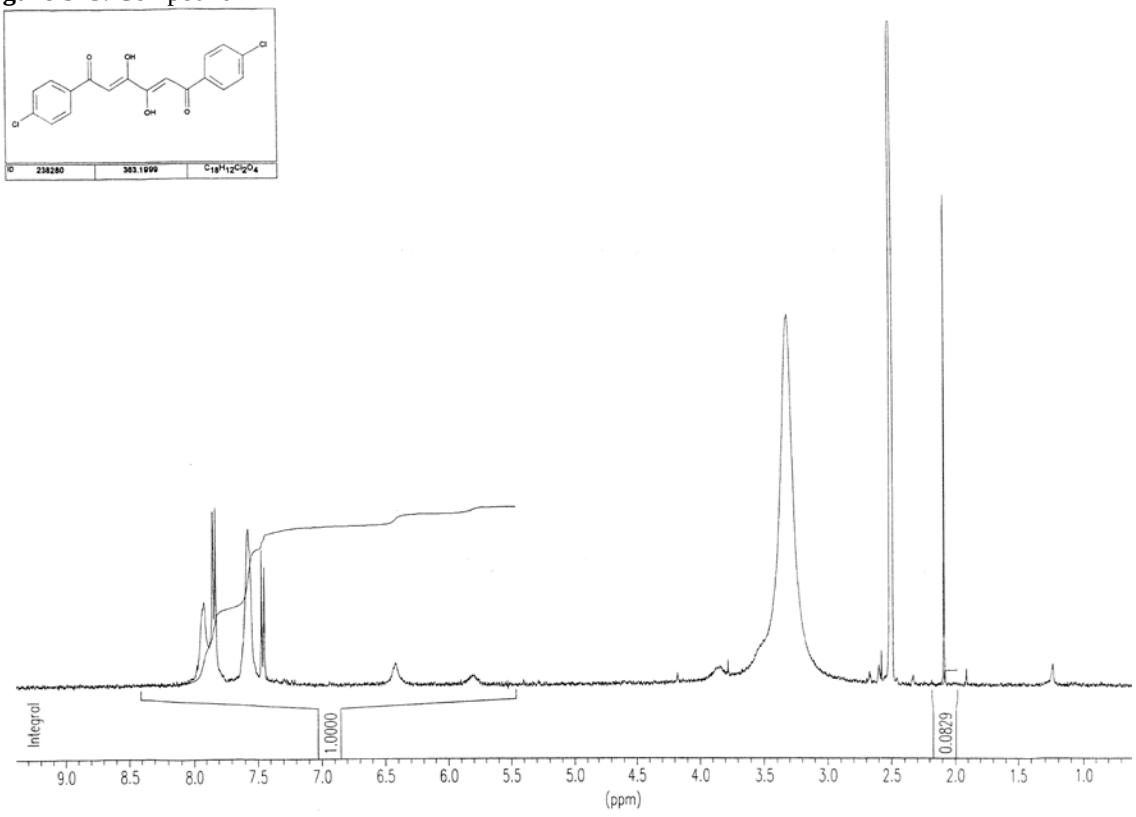

Figure S14. Compound 5

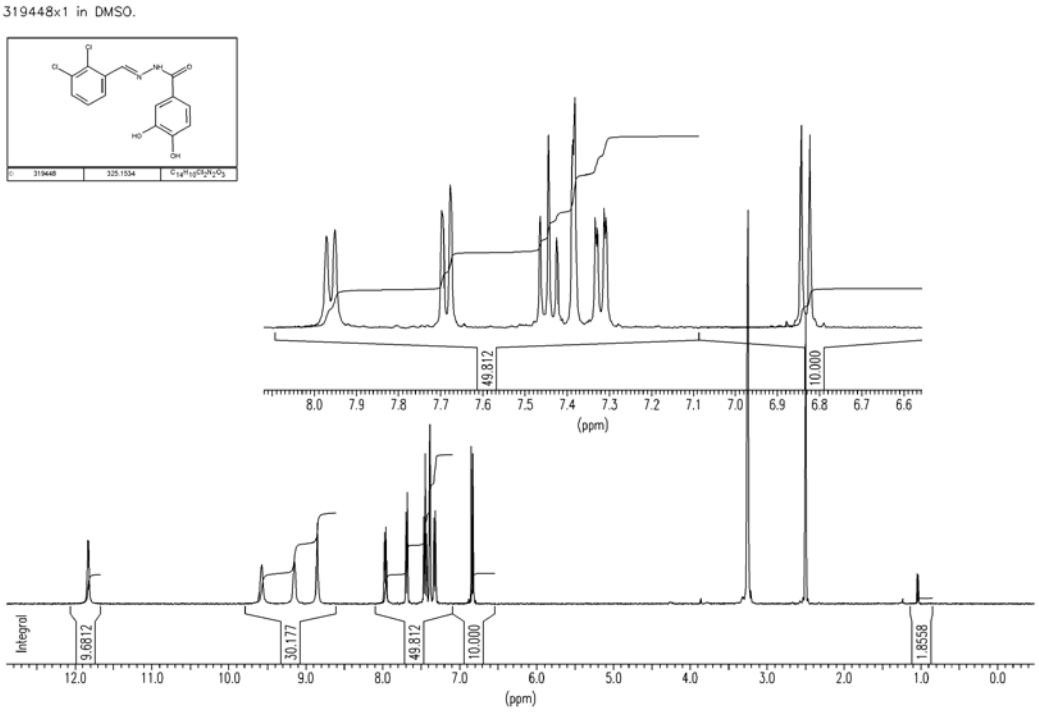

Figure S15. Compound 6

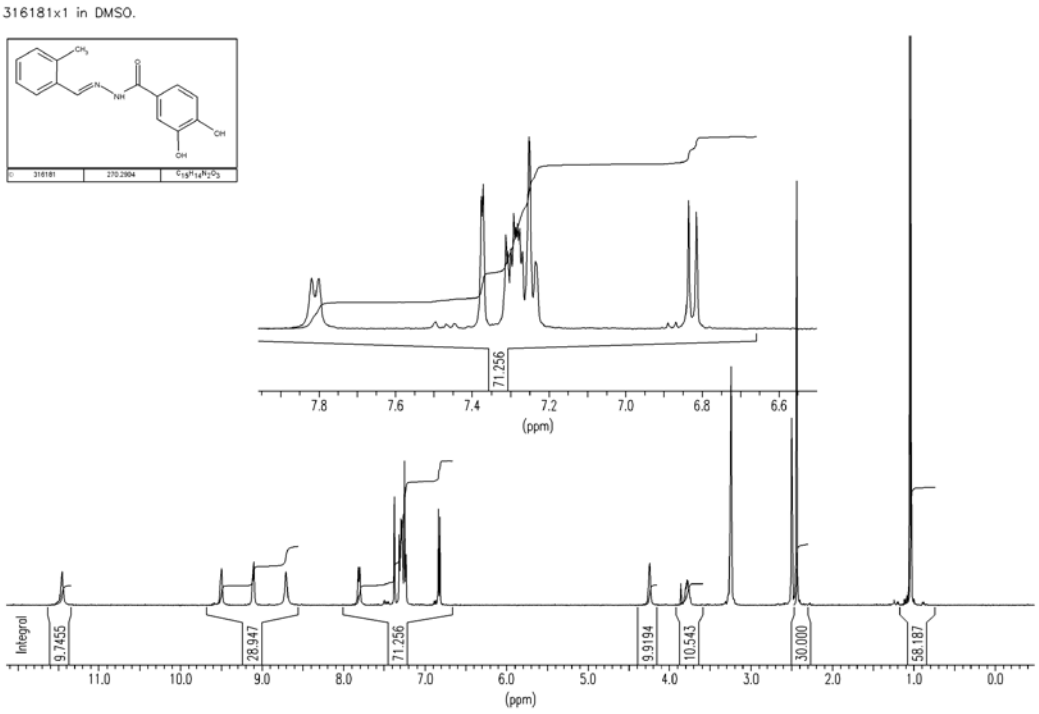

Figure S16. Compound 7

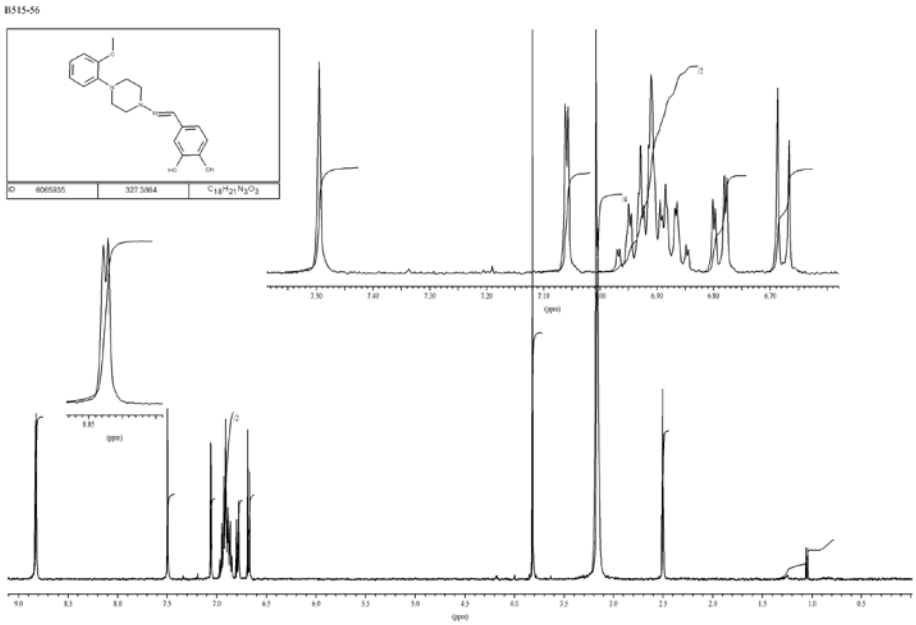

Figure S17. Compound 8

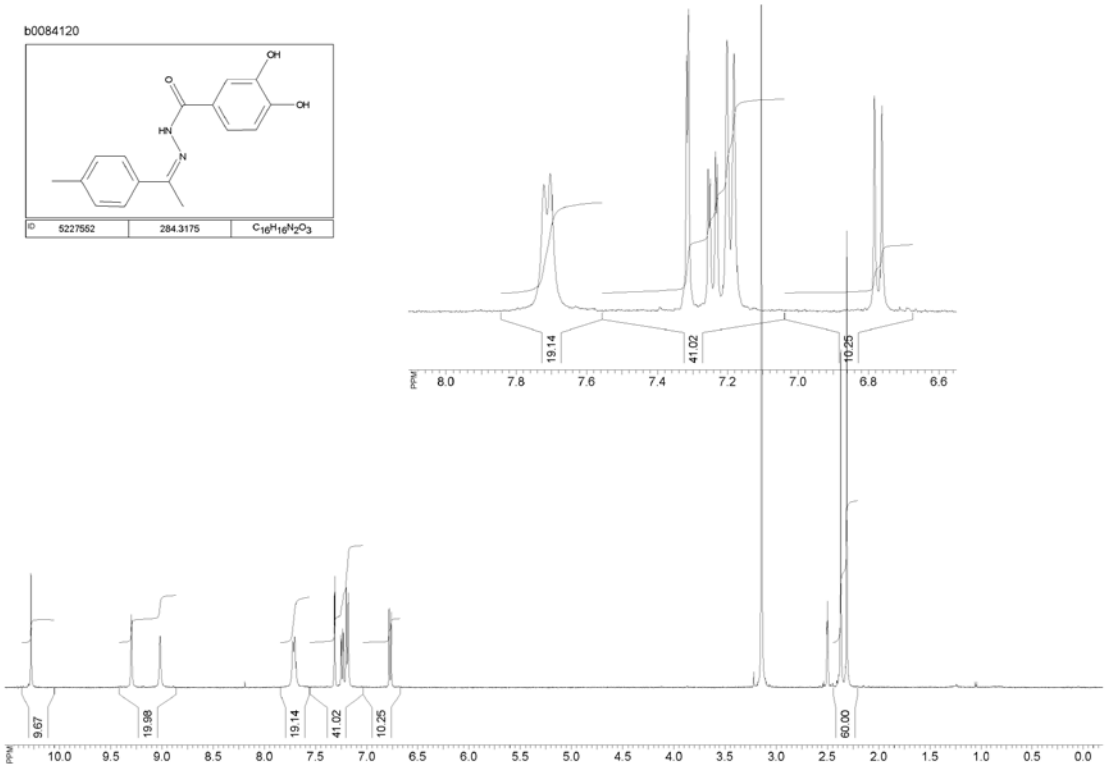

Figure S18. Compound 9

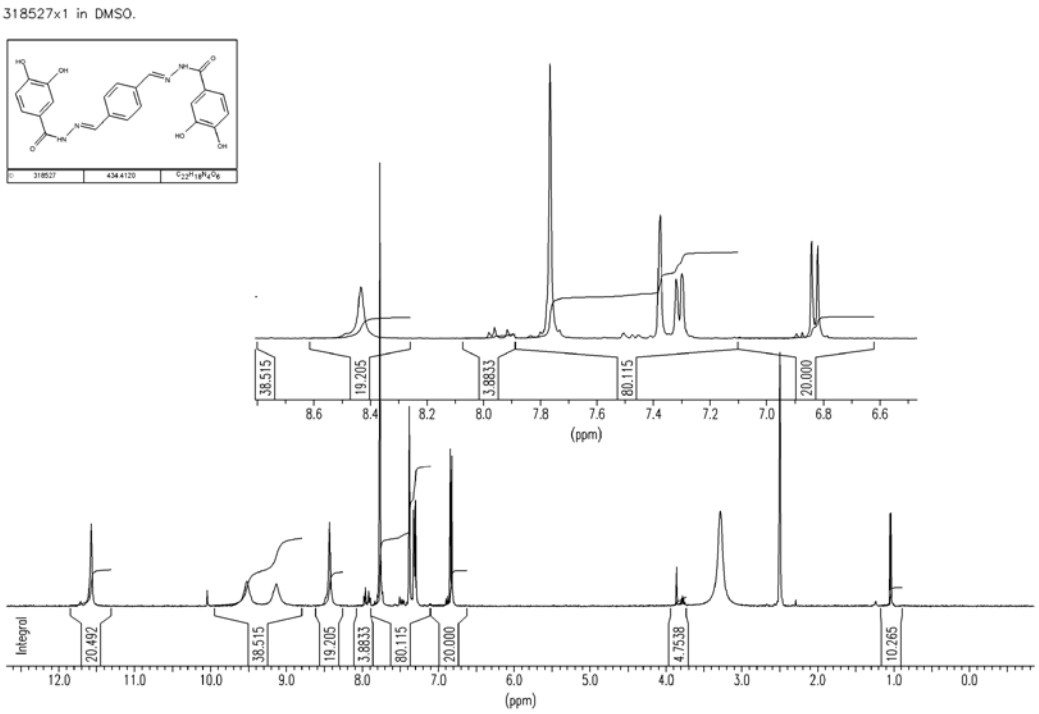

Figure S19. Compound 10

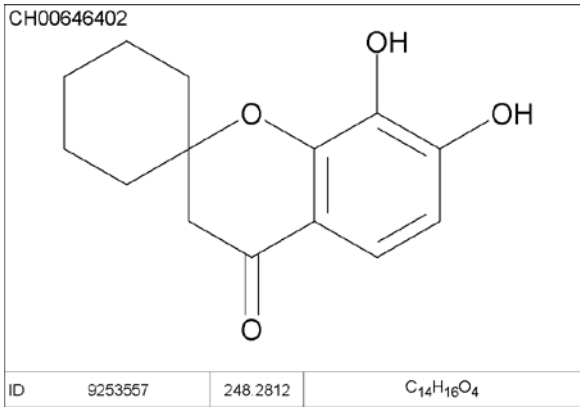


```
Data File D:\DATA\2173\1BA-0201.D
Sample Name: CH006464P1-B-01
Instrument 1 05/06/2010 04:22:23  #2
Column: Monolithic SpeedROD C18e 50x4.6mm |
3.75ml/min
Gradient: "A"->@2.1min->"B"(Hold 0.8min)-
>@0.2min->"A"->PostRun
PMP1, Solvent A         : 0.1%TFA in MeOH/H2O
(2.5:97.5)
PMP1, Solvent B         : 0.1% TFA in MeOH
PMP1, Solvent C         : 0.1%FA in ACN/H2O
(2.5:97.5)
PMP1, Solvent D         : 0.1%FA in ACN
Ionization mode             :    API-ES Positive

Signal 1: ADC1 A, ELSD
Peak RetTime Type  Width     Area      Height
Area
  #   [min]        [min]   [mV*s]      [mV]
%
----|-------|----|-------|----------|----------|-
-------|
   1   1.433 PV   8.78e-3    3.19372    6.44141
1.5604
   2   1.478 VB    0.0369  201.48332   76.04863
98.4396
Totals :                   204.67704   82.49004


Signal 2: DAD1 A, Sig=300,200 Ref=off
Peak RetTime Type  Width     Area      Height
Area
  #   [min]        [min]   [mAU*s]     [mAU]
%
----|-------|----|-------|----------|----------|-
-------|
   1   1.431 BP    0.0703 5806.34668 1373.78333
90.6964
   2   1.984 PP    0.0569  435.79807  115.91527
6.8073
   3   2.550 BPA   0.0458  159.81485   52.07167
2.4963
Totals :                  6401.95959 1541.77027


Signal 3: MSD1 TIC, MS File
Peak RetTime Type  Width     Area      Height
Area
  #   [min]        [min]
%
----|-------|----|-------|----------|----------|-
-------|
   1   1.485 PP    0.0635 2.94941e7  7.06214e6
100.0000
Totals :                  2.94941e7  7.06214e6
```

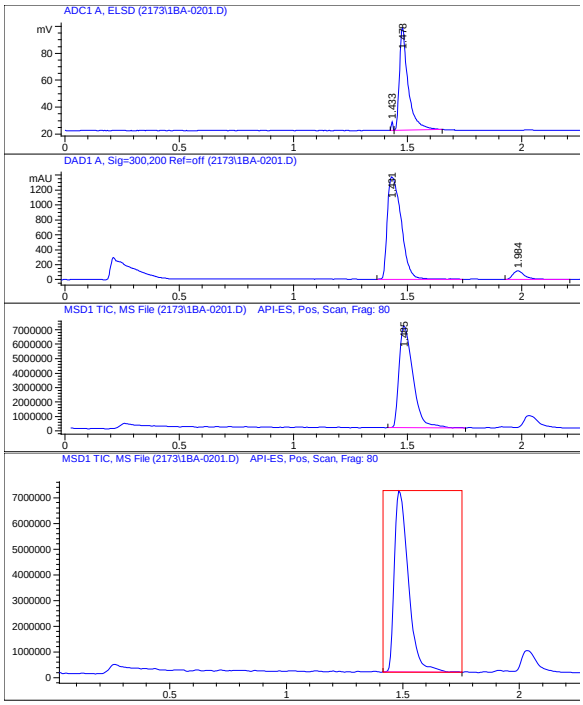

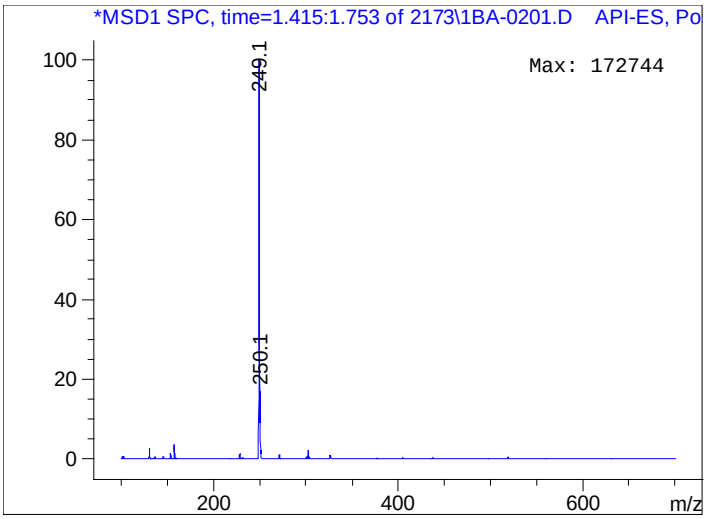

Figure S20. Compound 11

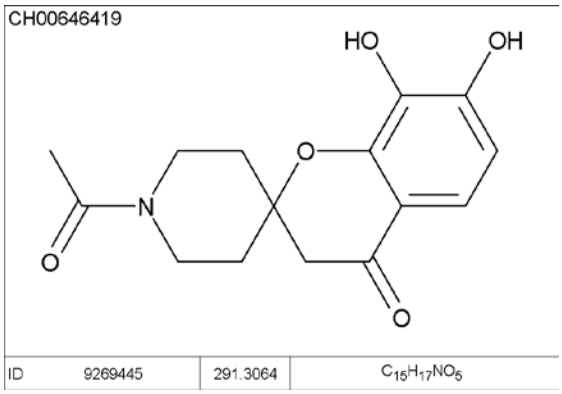


```
Data File D:\DATA\2173\1CC-1901.D
Sample Name: CH006464P1-C-03
Instrument 1 05/06/2010 05:34:32  #2
Column: Monolithic SpeedROD C18e 50x4.6mm |
3.75ml/min
Gradient: "A"->@2.1min->"B"(Hold 0.8min)-
>@0.2min->"A"->PostRun
PMP1, Solvent A          : 0.1%TFA in MeOH/H2O
(2.5:97.5)
PMP1, Solvent B          : 0.1% TFA in MeOH
PMP1, Solvent C          : 0.1%FA in ACN/H2O
(2.5:97.5)
PMP1, Solvent D          : 0.1%FA in ACN
Ionization mode              :    API-ES Positive

Signal 1: ADC1 A, ELSD
Peak RetTime Type  Width     Area      Height
Area
  #   [min]        [min]   [mV*s]      [mV]
%
----|-------|----|-------|----------|----------|-
-------|
   1   1.088 PB    0.0421  401.03699  141.42334
100.0000
Totals :                   401.03699  141.42334


Signal 2: DAD1 A, Sig=300,200 Ref=off
Peak RetTime Type  Width     Area      Height
Area
  #   [min]        [min]   [mAU*s]     [mAU]
%
----|-------|----|-------|----------|----------|-
-------|
   1   1.042 BB    0.0692 5962.38721 1414.19434
100.0000
Totals :                  5962.38721 1414.19434


Signal 3: MSD1 TIC, MS File
Peak RetTime Type  Width     Area      Height
Area
  #   [min]        [min]
%
----|-------|----|-------|----------|----------|-
-------|
   1   1.098 BP    0.0612 2.09176e7  5.25786e6
100.0000
Totals :                  2.09176e7  5.25786e6
```

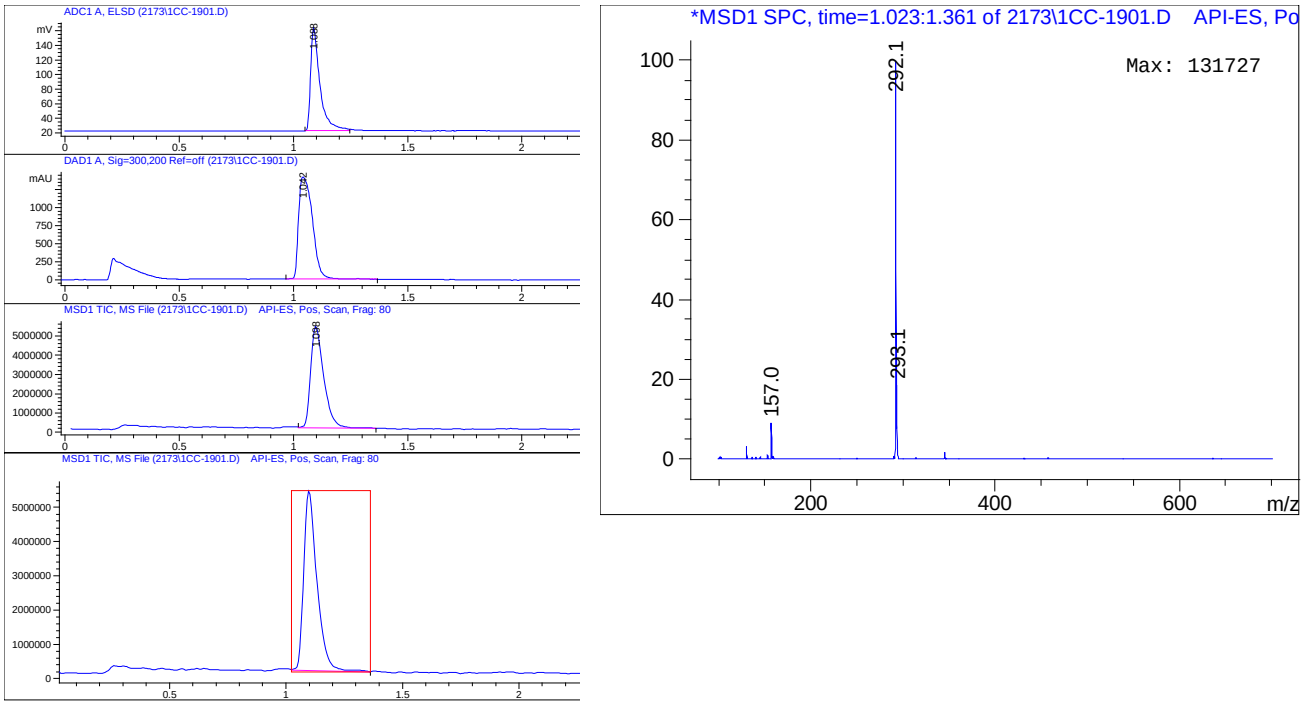

Figure S21. Compound 12

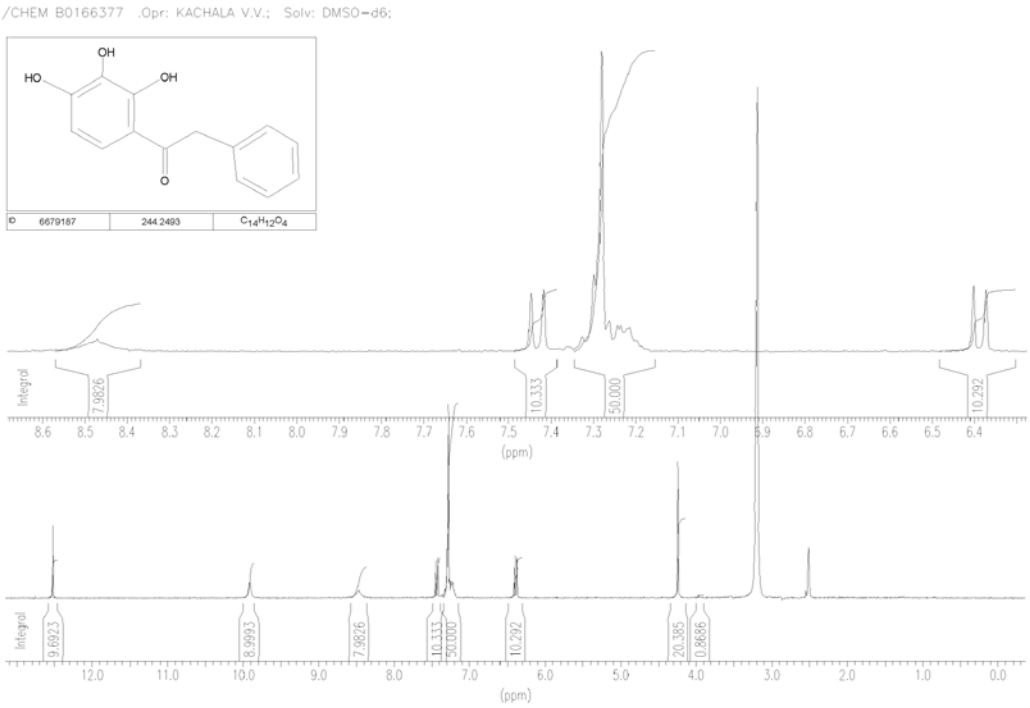

Figure S22. Compound 13

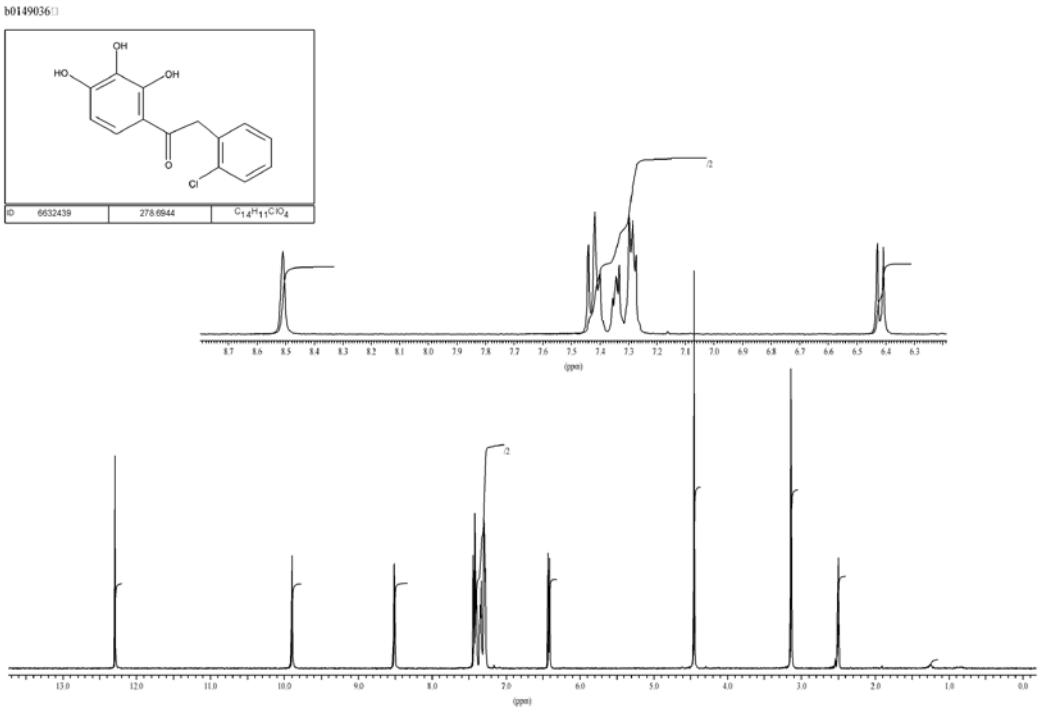

Figure S23. Compound 14

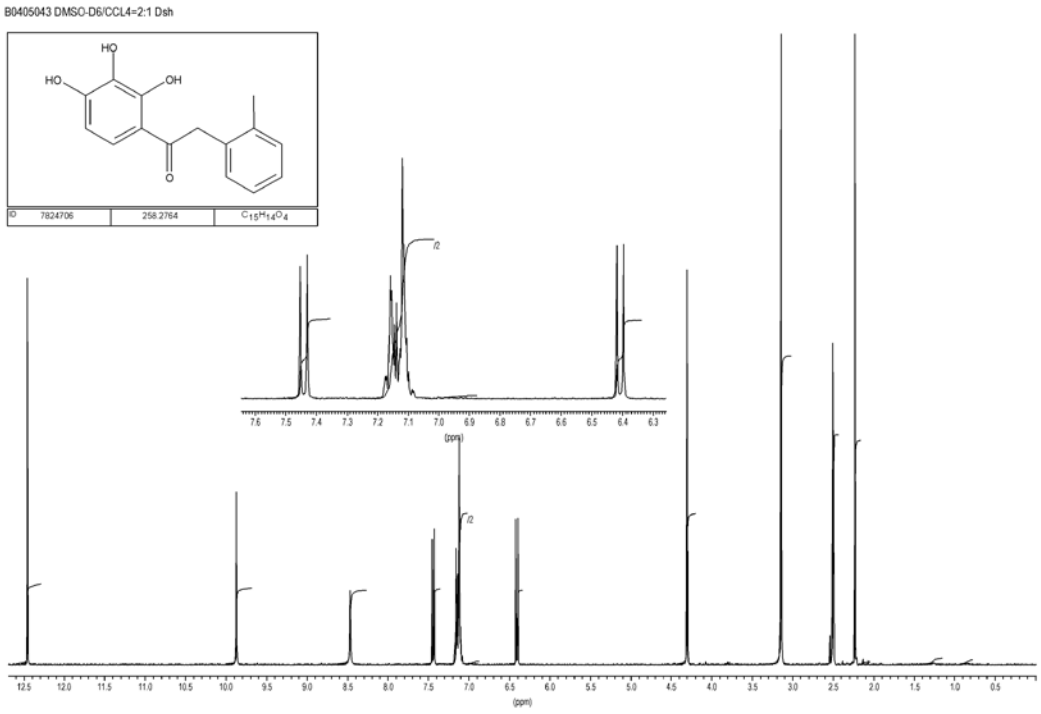

Figure S24. Compound 15

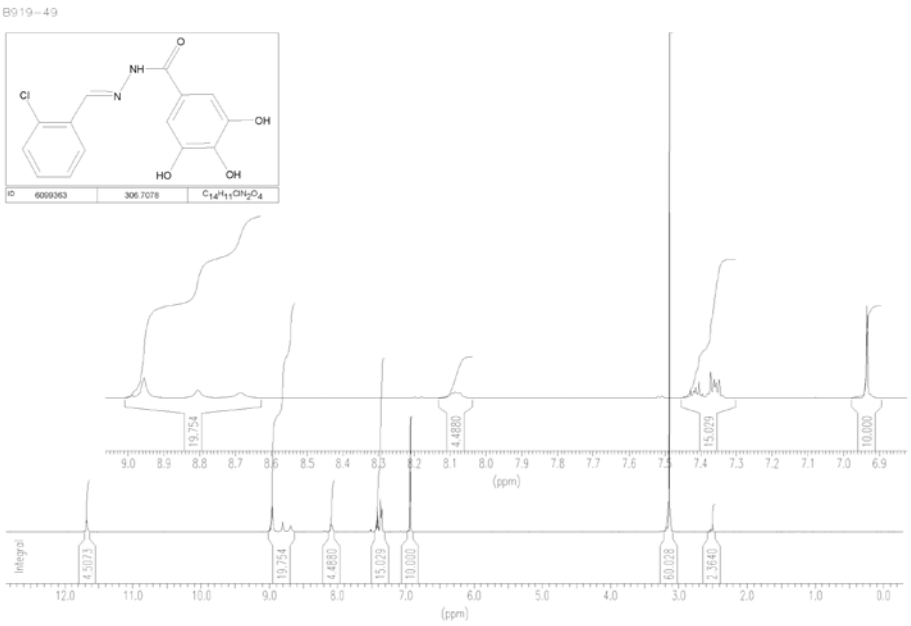

Figure S25. Compound 16

References

1 vROCS v, OpenEye Scientific Software, Inc., Santa Fe, NM, USA, http://www.eyesopen.com, 2011.
2 Maestro, version 9.3, Schrödinger, LLC, New York, NY, 2012.
3 W. Humphrey, A. Dalke, K. Schulten, *J. Molec. Graph.*, 1996, **14**, 33-38.
4 OMEGA v2.1, OpenEye Scientific Software, Inc., Santa Fe, NM, USA, http://www.eyesopen.com, 2010.
5 T. Fawcett, *Pattern Recog. Lett.*, 2006, **27**, 861-874.
6 FILTER v2.1, OpenEye Scientific Software, Inc., Santa Fe, NM, USA, http://www.eyesopen.com, 2010.
7 C.A. Lipinski, F. Lombardo, B.W. Dominy, P.J. Feeney, *Adv. Drug. Deliv. Rev.*, 2001, **46**, 3-26
8 Y. Iwai, H. Takahashi, D. Hatakeyama, K. Motoshima, M. Ishikawa, K. Sugita, Y. Hashimoto, Y. Harada, S. Itamura, T. Odagiri, M. Tashiro, Y. Sei, K. Yamaguchi, T. Kuzuhara, *Bioorg. Med. Chem.*, 2010, **18**, 5379-5390.
9 R.M. DuBois, P.J. Slavish, B.M. Baughman, M.K. Yun, J. Bao, R.J. Webby, T.R. Webb, S.W. White, *PLoS pathogens*, 2012, **8**, e1002830.
10 Kowalinski, E.; Zubieta, C.; Wolkerstorfer, A.; Szolar, O. H.; Ruigrok, R. W.; Cusack, S. Structural analysis of specific metal chelating inhibitor binding to the endonuclease domain of influenza pH1N1 (2009) polymerase. PLoS Pathog 2012, 8, e1002.
11 Macromodel, version 9.9, Schrödinger, LLC, New York, NY (2012)
12 Gaussian 09 M. J. Frisch, G.W. Trucks, H.B. Schlegel, G.E. Scuseria, M.A. Robb, J.R. Cheeseman, G. Scalmani, V. Barone, B. Mennucci, G.A. Petersson, H. Nakatsuji, M. Caricato, X. Li, H.P. Hratchian, A.F. Izmaylov, J. Bloino, G. Zheng, J.L. Sonnenberg, M. Hada, M. Ehara, K. Toyota, R. Fukuda, J. Hasegawa, M. Ishida, T. Nakajima, Y. Honda, O. Kitao, H. Nakai, T. Vreven, J.A. Jr. Montgomery, J.E. Peralta, F. Ogliaro, M. Bearpark, J.J. Heyd, E. Brothers, K.N. Kudin, V.N. Staroverov, R. Kobayashi, J. Normand, K. Raghavachari, A. Rendell, J.C. Burant, S.S. Iyengar, J. Tomasi, M. Cossi, N. Rega, J.M. Millam, M. Klene, J.E. Knox, J.B. Cross, V. Bakken, C. Adamo, J. Jaramillo, R. Gomperts, R.E. Stratmann, O. Yazyev, A.J. Austin, R. Cammi, C. Pomelli, J.W. Ochterski, R.L. Martin, K. Morokuma, V.G. Zakrzewski, G.A. Voth, P. Salvador, J.J. Dannenberg, S. Dapprich, A.D. Daniels, Ö. Farkas, J.B. Foresman, J.V. Ortiz, J. Cioslowski, D.J. Fox, Gaussian, Inc., Wallingford CT, 2009.
13 (a) Schrödinger Suite 2013 Protein Preparation Wizard; (b) Epik version 2.3, Schrödinger, LLC, New York, NY, 2013; (c) Impact version 5.8, Schrödinger, LLC, New York, NY, 2013; (d) Prime version 3.1, Schrödinger LLC, New York, NY, 2013; (e) G.M. Sastry, M. Adzhigirey, T. Day, R. Annabhimoju, W. Sherman, *JCAMD*, 2013, **27**, 221; (e) M.H.M. Olsson, C.R. Sondergard, M. Rostkowski, J.H. Jensen, *J. Chem. Theor. Comput.*, 2011, **7**, 525-537.
14 MarvinSketch 5.11.4, 2012, ChemAxon (http://www.chemaxon.com).
15 (a) Glide, version 5.9, Schrödinger, LLC, New York, NY, 2013; (b) R.A. Friesner, J.L. Banks, R.B. Murphy, T.A. Halgreen, Klicic J.J., D.T. Mainz, M.P. Repasky, E.H. Knoll, M. Shelley M., J.K. Perry, D.E. Shaw, P. Francis, P.S. Shenkin, *J. Med. Chem.*, 2004, **47**, 1739-1749; (c) T.A. Halgreen, R.B. Murphy, R.A. Friesner, H.S. Beard, L.L. Frye, W.T. Pollard, J.L. Banks, *J. Med. Chem.*, 2004, **47**, 1750-1759.